PHY 451: Advanced Laboratory
Manual for Diode Laser Spectroscopy

Derek Neben, Lennart Dabelow

Department of Physics & Astronomy
Michigan State University
East Lansing, MI 48824

Motivation

The general idea of this experiment is to study the interaction of light and matter using the example of resonant absorption in rubidium. Our light source is a diode laser, which provides a coherent beam of almost one frequency with a very narrow bandwidth. This frequency is tunable within a certain range around $384\,\mathrm{THz}$ ($780\,\mathrm{nm}$), matching with the D2 transitions (from the $5\mathrm{S}_{1/2}$ to the $5\mathrm{P}_{3/2}$ energy levels) in 87Rb and 85Rb isotopes.

Diode Laser and Mode Hopping

The diode laser uses a semiconductor chip similar to a light emitting diode (LED) to produce infrared laser light. This chip is housed in an optical trap to facilitate stimulated emission with one mirror slightly transmitting the light. The light passes out of the laser cavity onto a diffraction grating at an angle to the incident beam, allowing the transmission of a specific frequency. Light intensity is proportional to the current across the diode, furthermore the laser will not produce coherent light (in other words operate as an LED) until a threshold is reached (threshold current) and the laser will lase. Light produced from the laser is coherent, linearly polarized, and narrow bandwidth (approximately 50 Mhz [1]).

Mode hopping abruptly changes laser properties, manifesting by breaking the absorption spectrum as traced on an oscilloscope, and making positive identification of ground state splitting difficult. Fortunately simultaneous modulation of laser current and diffraction grating angle can minimize this effect and will be covered in the single beam absorption experiment.

Hyperfine Splitting of Rubidium

You will be measuring the hyperfine splitting of 85Rb and 87Rb using absorption spectroscopy. The rubidium atom's valence electron will be excited from the $5\mathrm{S}_{1/2}$ to the $5\mathrm{P}_{3/2}$ state with application of light at 780.2nm. This is true because the coulomb attraction on the electron cloud for each isotope is identical. However, these atoms have a hyperfine perturbation to the electronic states from the interaction between nuclear and electron magnetic moments. Hyperfine splitting is the result of coupling between the valence electron's and the nucleus' angular momenta. 85 and 87 rubidium have spin quantum numbers of 5/2 and 3/2 respectively resulting in greater magnitude of energy splitting for 87 rubidium, this is represented graphically in figure 1.

Please note that both the ground state ($5S_{1/2}$) and the first excited state ($5P_{3/2}$) exhibit splitting. Both isotopes share the same electronic transition and a common origin may be used to compare and identify each isotope.
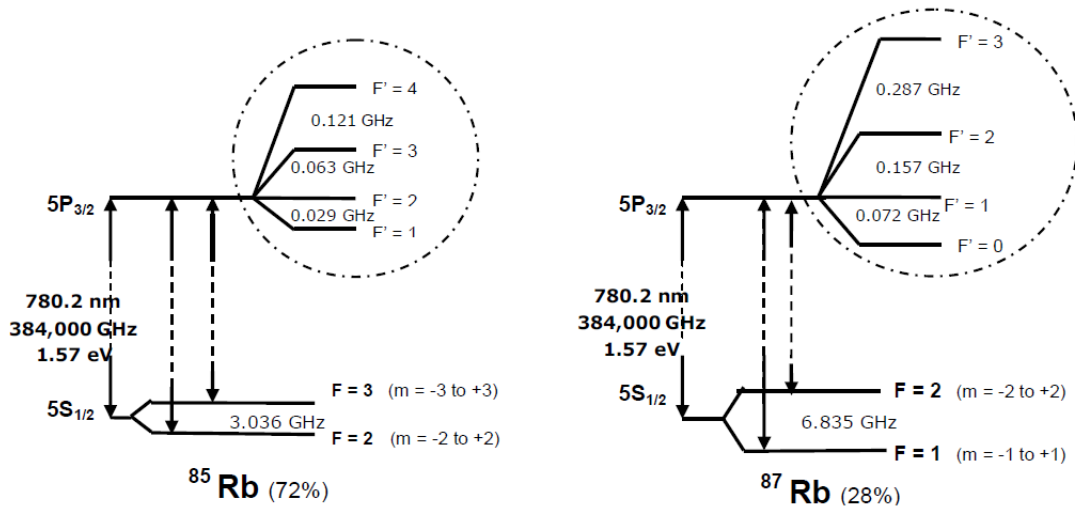
Figure 1: Hyperfine splitting of 85 and 87 rubidium[1]

Overview of the Experiments

Here is a summary of the experiments covered in this manual.

You may explore the properties of the diode laser and get a first qualitative picture of the absorption in the rubidium cell. You will **align the laser** to provide a stable beam of light, and you will observe **fluorescence** in the rubidium cell indicating the absorption and re-emission of photons by the atoms in the cell. You will also familiarize with the capabilities of the laser diode controller to scan the frequency spectrum automatically within a certain range, which is achieved by modulating the voltage across a piezo crystal at the mount of the diffraction grating. Depending on the grating angle, light of a specific wavelength is selected to be fed back to the laser cavity, which eventually becomes the emission frequency of the laser due to self-resonance.

In order to do spectroscopy, i.e. to measure frequency or energy differences in the energy splitting of rubidium, you would like to establish a relationship between the voltage applied to the piezo controller and the output frequency of the laser. Fortunately, we find the change in frequency to be directly proportional to the change of the ramp voltage used for the automated frequency scan, so we can describe the correlation by a constant C_{ramp}. We suggest to set up a **Michelson interferometer** to obtain a first estimate of its value. The alignment is relatively simple, and you will be able to discover some more characteristics of the laser.

Once familiar with the diode laser, you are ready to start with the actual absorption experiments. You may begin with **single beam absorption**. You will find the typical resonance peaks resembling the hyperfine splitting of the $5S_{1/2}$ energy levels of 87Rb and 85Rb isotopes. However, these peaks are significantly broadend by means of the Doppler effect: due to thermal energy, the atoms in the cell are not at rest, but rather floating around at different velocities, such that they "see" the incident light slightly shifted in frequency. So while the hyperfine splitting of the $5S_{1/2}$ level is in the range of 3 to 7 GHz, the structure of the $5P_{3/2}$ levels is blurred by Doppler broadening since they split into sub-levels with distances between 0.03 and 0.3 GHz.

However, you may increase the resolution dramatically by extending the experimental setup. You will use a second beam of higher intensity passing through the cell in the opposite direction to the first. The **saturated absorption** technique takes advantage of the fact that the atoms in the cell will see the opposing beams shifted to different frequencies and will therefore interact with only one of them, unless their velocity vanishes.

---

[1]Source: [1, p. 2-8]

In this case, the strong beam excites most of the atoms in the cell, and the weaker beam will be absorbed less.

After obtaining a high-resolution picture of the hyperfine splitting of the rubidium D2 transition, you may notice that the precision of the automated frequency scan calibration above using a simple Michelson interferometer was not high enough to actually measure the energy levels reliably. Therefore, you may set up the provided **Fabry-Pérot interferometer**. Using a radio-frequency modulation of the laser light, it will allow you to determine the ramp constant with significantly higher accuracy. Furthermore, you will be able to observe resonance absorption and measure frequencies simultaneously.

Finally, you may go on to your own research project and explore other effects such as the influence of an external magnetic field or refractive index measurement.

1 Laser Alignment and Fluorescence

The first step in obtaining an absorption spectrum with the diode laser is to observe fluorescence of the rubidium vapor, because when the vapor is fluorescing it is absorbing light and will therefore lower the transmission of laser light providing a contrast that may be measured. Observation of fluorescence is critical for future success in this experiment series.
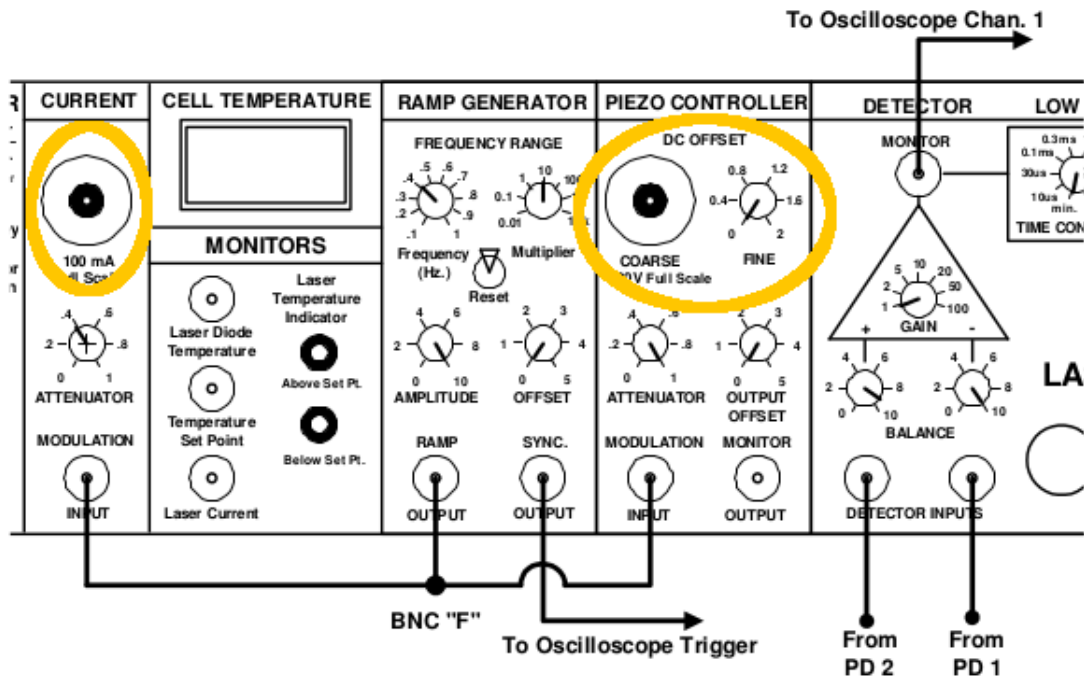

Figure 2: TeachSpin laser diode controller front panel. Highlighted are the laser current and defraction grating angle controls, left and right respectively[2]

The TeachSpin laser diode controller adjusts the three primary laser parameters, temperature, current, and diffraction grating angle. To turn on the control unit flip the master power switch in the rear of the unit by the power input. The unit will begin to maintain laser diode and rubidium cell temperature to set

---

[2]Source: [1, p. 3-15]

point. The laser temperature set point was determined by the manufacturer to be 2.728 V (corresponding to approximately 21 °C) as read from the laser diode temperature monitor by multimeter. It may be changed on the rear of the control panel using the potentiometer dial. Laser current and diffraction grating angle may be changed using the potentiometer knobs on the control panel face as indicated in fig. 2. The laser current can be monitored by multimeter from the laser current monitor on the front panel. 1 V on the multimeter corresponds to a current of 10 mA. The rubidium cell temperature should be maintained at 60 °C as read from the cell temperature monitor. For adjustment, please refer to the TeachSpin manual[1, p. 5-27].

The various experimental setups are constructed on an optical breadboard. To conduct optical absorption spectroscopy, the experiment is set up as shown in fig. 3. The suggested layout is constructed to facilitate implementation of subsequent experiments. The requirement to observe fluorescence is simply that light is passed through a vapor cell at the correct frequency. The absorbed light may then be re-emitted by the rubidium atom in any direction and allows for observation transverse to beam direction by the video camera.
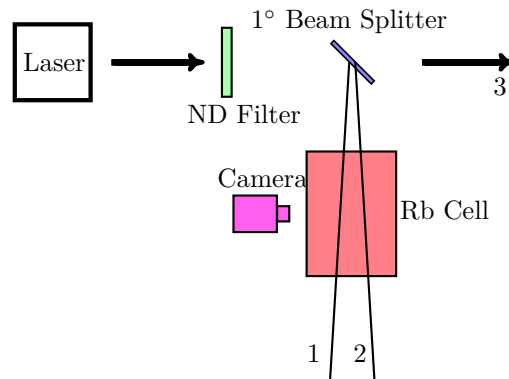

Figure 3: Basic components to observe fluorescence

The basic components in this experiment are the diode laser, ND filter, 1° 10:90 beam splitter, video camera, and rubidium cell. The ND filter's purpose is to prevent the propagation of incoherent light from the laser (after all the laser will operate like an LED below threshold). The beam splitter will reflect a portion of the laser beam (one reflection of each surface), and this beam splitter is ground as a wedge and will provide diverging reflected beams. These beams should be directed through the rubidium cell. As shown in fig. 3 beams 1 and 2 reflected by the beam splitter are detectible using the Teachspin observing card, and beam 3 is unused in this experiment. The video camera is used to observe rubidium fluorescence because IR light is invisible to the human eye.

1.1   Procedure

The first step in this experiment is to lase the laser, or to produce a laser beam. This is easily accomplished by increasing the laser current to above a threshold value wherein the light emitting diode will transcend into stimulated emission. Conformation of lasing may be performed with the provided infrared observation card. Alternatively, a photodiode detector may be placed in the beam path and monitored with the oscilloscope. Rough knowledge of the threshold current will provide you with a reference point when performing future experiments, it is typically around 32 mA.

1. Begin operating the laser by turning the laser current to above the threshold value as previously found. Fluorescence may be observed simply by increasing laser current (see fig. 4), if this is the case then you should take this opportunity to learn how to sweep the diffraction grating angle by adjusting the voltage across the piezo stack, and the laser current.

2. Sweep of the voltage across the piezo stack is easily achieved using the TeachSpin laser control box and

Figure 4: Fluorescence as observed on the monitor

its implementation is described on page 3-8, section E, parts 3 and 4 of [1]. The piezo sweep range may be changed by the DC offset function.

3. Now you may connect the ramp output to the current modulation input on the laser diode controller front panel as shown on p. 3-14 (section I, parts 1 through 3) of the TeachSpin manual[1]. This reduces mode hopping of the diode laser, as observed in future experiments.

4. Fluorescence is observed at a laser current of around $52\,\mathrm{mA}$ and a piezo voltage range between 3 and $8\,\mathrm{V}$ for a rubidium cell temperature of $60\,^{\circ}\mathrm{C}$.

If upon scanning many current and voltage combinations fluorescence is still not observed it is possible the diode laser cavity is misaligned. The alignment procedure is presented between pgs. 3-4 and 3-14 of the TeachSpin manual[1].

2   Michelson Interferometer

The aim of this section is to explore basic properties of the laser such as the frequency dependence upon grating angle and laser current. Furthermore, you will lay the foundations for future quantitative measurements of the rubidium absorption spectrum by calibrating the apparatus.

2.1   Setup

This experiment is independent of the absorption experiments, so in principle, you can set it up anywhere on the optical table. However, we recommend to leave the 10/90 beam splitter in place and use the probe beam as the input to the interferometer. You will need the 10/90 beam splitter in this position for the saturated absorption experiment. The beam should not pass through the rubidium cell. Therefore, you may unscrew the cell and put it aside. You can leave the coils in place, though, and let the beam pass through the coils.
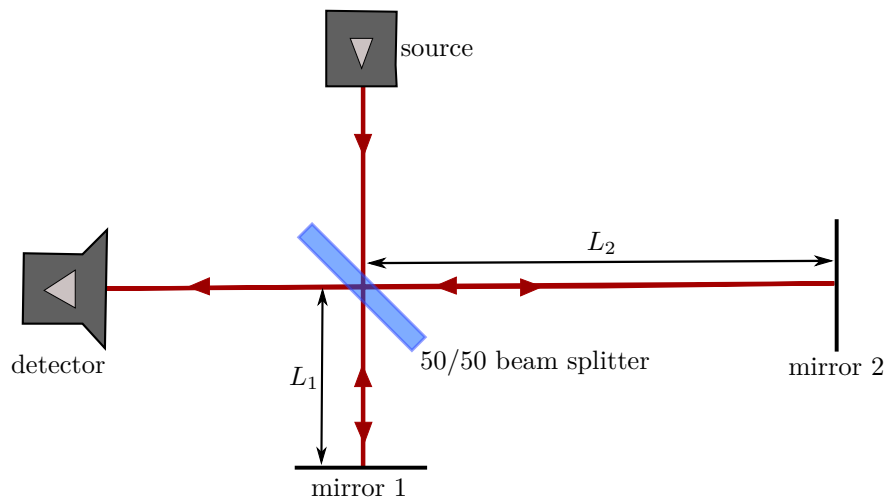
Figure 5: Michselson interferometer outline

The heart of the Michselson interferometer is the 50/50 beam splitter in the center, which splits the incident beam into two separate paths of different lengths and recombines them again afterwards. You may use the filter holder (no adjustment screws) for the 50/50 beam splitter to allow the beams to pass through in all directions. Also, you would like to have the difference between the two paths to be as long as possible for better precision. Thus keep one mirror close to the beam splitter, and make sure you have enough space for the second mirror.

You may follow the instructions in the TeachSpin manual[1], pp. 3-26 through 3-28. The crucial point is to get the beams collinear. Do not modulate the piezo voltage and laser current during alignment. You should be able to see a fringe pattern on the business card screen with the video camera before adding the photodetector.

When the beams are aligned, you may restart the frequency scan and watch the signal on the oscilloscope. Compare the differences between independently scanning the piezo voltage and the laser current, and modulating both simultaneously. The final signal on the 'scrope should look similar to fig. 6, maybe you can get it even better.

2.2 Calibration of the Frequency Scan Using a Michelson Interferometer

For a Michelson interferometer as in fig. 5, we will find a maximum of intensity whenever the optical path difference $\delta = 2|L_1 - L_2|$ is an integer-multiple of the wavelength:

$$\delta = m\lambda \qquad (m \in \mathbb{N}_0). \tag{1}$$

Try to measure the lengths of the two paths L_1 and L_2 as precise as possible, for example using twine. This will allow you to establish a relation between the change of ramp voltage ΔV used to modulate the piezo control and laser current, and the corresponding change of the laser frequency $\Delta \nu$. Using $\lambda = c/\nu$, it follows from eq. (1) that we will find maxima of intensity whenever

$$\nu = \frac{c}{\delta}m.$$

Thus, if we have two intensity maxima with a difference of orders Δm, i.e. Δm peaks between the two considered maxima, the change in frequency $\Delta \nu$ between these two maxima is therefore
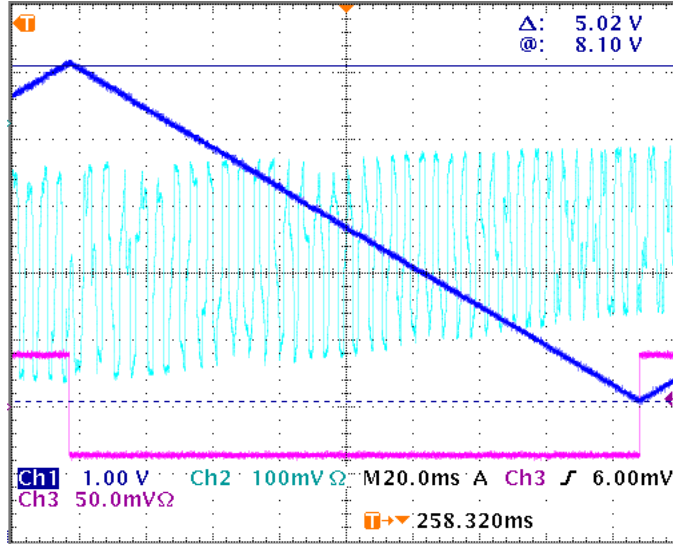
$$\Delta \nu = \frac{c}{\delta}\Delta m. \tag{2}$$

Figure 6: Example of the interference pattern obtain from the Michelson interferometer.
Blue: piezo voltage. Turquois: detector signal. Pink: trigger signal.

Monitoring the piezo voltage and the detector signal simultaneously, we can correlate the distance between the maxima Δm to a voltage change ΔV, defining $V_m = \Delta V / \Delta m$. Inserting this into eq. (2) yields

$$\Delta \nu = \frac{c}{\delta V_m} \Delta V = C_{\mathrm{ramp}} \, \Delta V \,, \qquad C_{\mathrm{ramp}} = \frac{c}{\delta V_m} \,. \tag{3}$$

This relation will permit us to measure the energy differences in the hyperfine structure of rubidium.

Note that due to the coarse measurement of the path lengths, there is a relatively high uncertainty for the obtained frequency differences. Nevertheless, the accuracy can be improved tremendously by using a Fabry-Pérot interferomenter (see below).

3   Single Beam Absorption

This experiment will utilize a photodiode detector to measure the light intensity of incident light sources, and with this device a spectrum may be traced on an oscilloscope. This spectrum will allow identification of specific isotopes of rubidium, but Doppler broadening will reduce the precision of the instrument.

3.1   Optical Layout

The optical table layout used is nearly identical to that used to observe fluorescence. In order to quantitatively measure the absorption spectrum an optical detector is placed downrange of the rubidium cell to interact with one of the two beams reflected off of the beam splitter as shown in figure 7. Attach the output of the detector directly into your oscilloscope, and replace the rubidium cell removed during the interferometry experiment. Also, you will not need the 50/50 beam splitter.
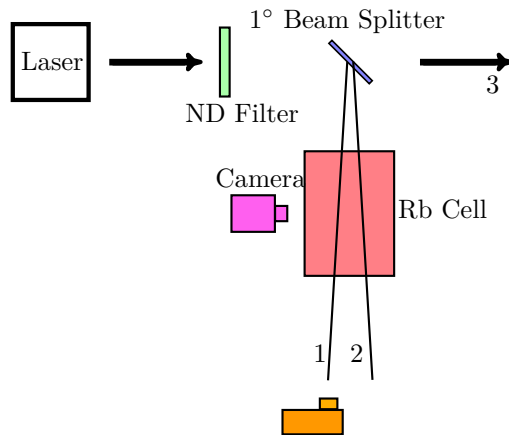
Figure 7: Optics components to observe rubidium absorption spectrum

Be sure to place the right or left handed photodiode detector on the left or right beams to facilitate setup of the following experiment, saturated absorption spectroscopy.

3.2   First Measurement

Similarly to fluorescence it is advantageous to keep the range of voltages swept across the piezo stack to be a maximum because this will provide the largest frequency bandwidth to interact with the rubidium vapor. Sweeping the piezo stack for a finite diode junction current and temperature will produce an absorption spectrum as shown in fig. 8.

The four clear absorption peaks observed in fig. 8 correspond to the $5S_{1/2}$ hyperfine splitting in 85 and 87
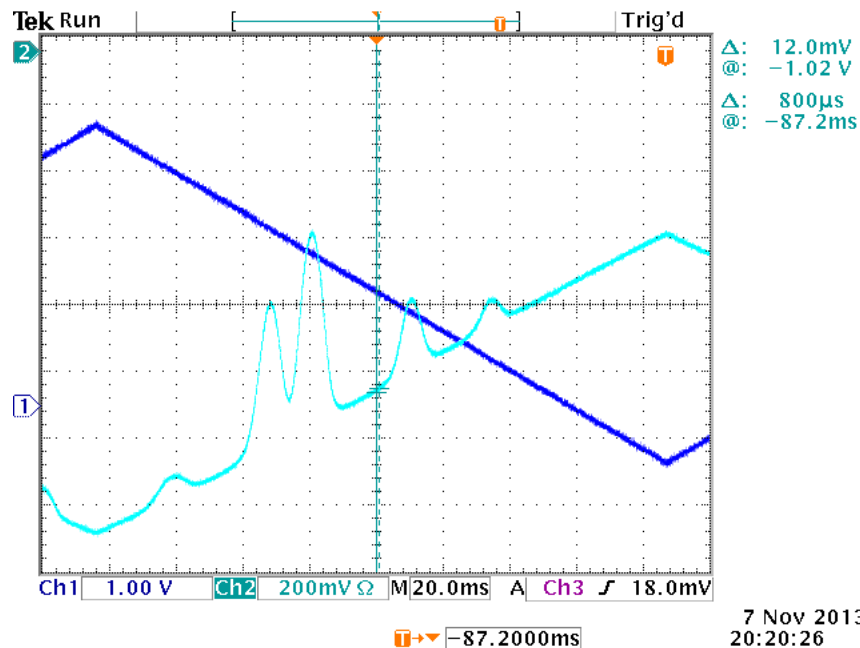

Figure 8: Absorption spectrum of Rubidium sweeping both current and grating angle

8

rubidium. The isotope 87 rubidium exhibits a larger magnitude of hyperfine splitting than 85 rubidium in the ground state ($5S_{1/2}$).

To see how the simultaneous modulation of the piezo voltage and laser current helps to reduce mode hopping, unplug the ramp generator from the current modulation input. The result should look similar to fig. 9, the spectrum is now littered with mode hopping by the diode laser. The mechanism of the simultaneous modulation is described on page 3-14, section I., parts 1 through 3 of [1]. Furthermore cleaner adsorption spectra may be obtained by tuning the piezo DC offset, detector gain, and laser current.
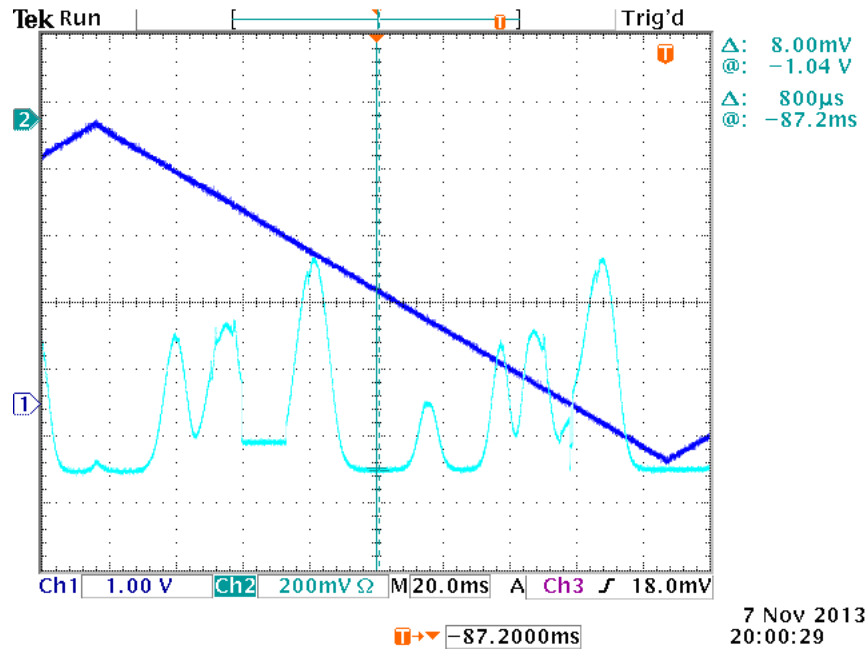

Figure 9: Absorption spectrum of Rubidium with sweep of diffraction grating angle only

The quantum mechanical transitions are discrete but figure 8 exhibits a continuous absorption curve, and this structure is due to Doppler shifting of the incident laser light from thermal motion in the rubidium vapor. In the atomic frame the vapor will "see" laser light blue or red shifted depending on the velocity of a rubidium atom. Doppler broadening is proportional to temperature, i.e. the colder the vapor, the narrower the bandwidth of the absorption spectrum and the sharper the measurement. However there is an alternative method that will be introduced in the following experiment that will induce stimulated emission for atoms that are neither blue nor red shifted in other words, atoms whose velocity is directed transverse to the incident laser beam path.

From knowledge of hyperfine splitting the signatures of isotopes 85 and 87 Rb may be identified qualitatively. You can use the calculated C_{ramp} from the Michelson interferometer experiment to measure the energy splitting quantitatively. Compare to the reference values as indicated in fig. 1.

4   Saturated Absorption Spectroscopy

Saturated absorption uses two beams to minimize the effect of Doppler shifting on the absorption of rubidium in the cell. As was setup previously, the first beam, called probe beam, is passed through the rubidium cell to measure a spectrum which interacts with a population of atoms shifted into and at resonance. Now if a second beam, the so-called pump beam, were passed through from the reverse direction and of greater
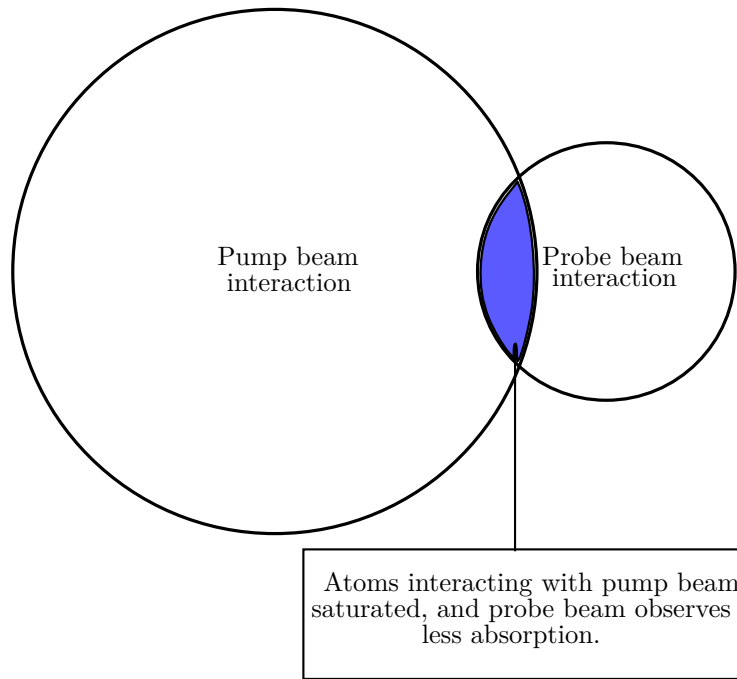
Figure 10: Cartoon of colinear cross-beam interaction populations of rubidium vapor

intensity than the probe beam, it will interact with a *mostly* different population of atoms shifted into and at resonance. Atoms that interact with *both* the pump and probe beams will absorb less than other populations and a distinct peak is observed, figure 10 illustrates this idea.

If the two beams were allowed to interact collinearly the pump beam saturates atoms in the rubidium cell and will not absorb the probe beam at the shared frequency. Both the pump and probe beams will interact with the same atoms when the vapor velocity is directed perpendicular to the incoming beams. This small population of atoms are saturated into excited states by the pump beam and therefore absorb less of the probe beam's light, and stimulated emission will even increase the number of photons reaching the detector. In other words the pump beam reduces the number of available absorbing atoms for the probe beam at the mutually shared frequency, and the error due to Doppler broadening is compensated.

4.1   Optical Layout

The reason a mostly transparent beam splitter was used in previous experiments was to allow for easy implementation of the pump and probe beams in saturated absorption spectroscopy. The optical table should look similar to figure 11 where mirrors and a 50:50 beam splitter have been added along with a second detector. The 50:50 beam splitter should only interact with one of the beams coming from the 1° beam splitter. The second of these two beams, which we will refer to as the reference beam, may allow you to electronically subtract the slope in the spectrum obtained from the current modulation.

Hookup your detectors as described on page 3-15, section J of the TeachSpin manual[1], note that you do not want to replicate their optical table layout only the detector hookup scheme.
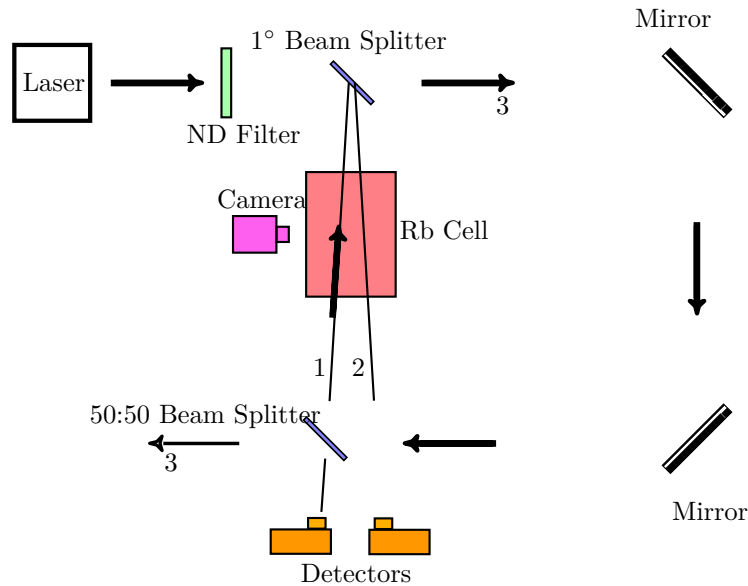
Figure 11: Optical table layout for SAS

4.2 Measurement

With a multitude of optical components, some interacting collinearly, it is important to take care when performing alignment. It is recommended to begin by aligning the mirrors to roughly transmit the pump beam onto the 50:50 beam splitter (which should be removed from the filter holder and placed in a mirror mount). It is important to make sure the pump and probe beams are collinear during this experiment, and optimization may begin once both the probe and pump beams are transmitted through the rubidium cell. Tuning may be performed by aligning components in the order of up range to down range with respect to the diode laser. Coarse adjustment may be performed with the IR viewing card while fine adjustment should be performed while measuring spectra with the oscilloscope. Further recommendations on laser alignment may be found on page 3-21, sub section D of the TeachSpin manual[1].

Measurement of a SAS spectrum is obtained in a manner similar to that with single beam absorption. Both the laser diode current and piezo voltage should be modulated to reduce mode hopping. An example of what should be observed is presented in figure 12.

Again as with the previous experiment, you would like to measure the hyperfine splitting of the $5S_{1/2}$ levels, which were observed before. Closely inspecting the SAS peaks should reveal they are composed of several distinct elements which is hyperfine splitting of the $5P_{3/2}$ levels. Figure 13 zooms in on the leftmost peaks in figure 12 to explicitly show this effect. Comparison of the SAS spectra with figure 1 will assist in identification of the resonance peaks. However, the limited precision of the simple Michelson interferometer does not allow a reliable measurement of $5P_{3/2}$ splitting. Therefore, you might want to implement the Fabry-Pérot interferometer to achieve a more precise estimate of the ramp modulation constant C_{ramp}.
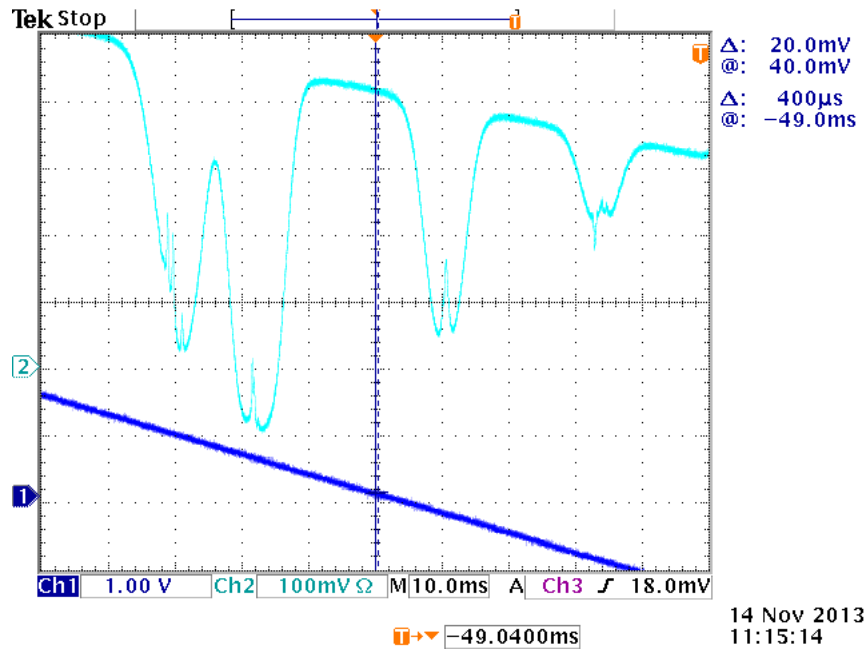
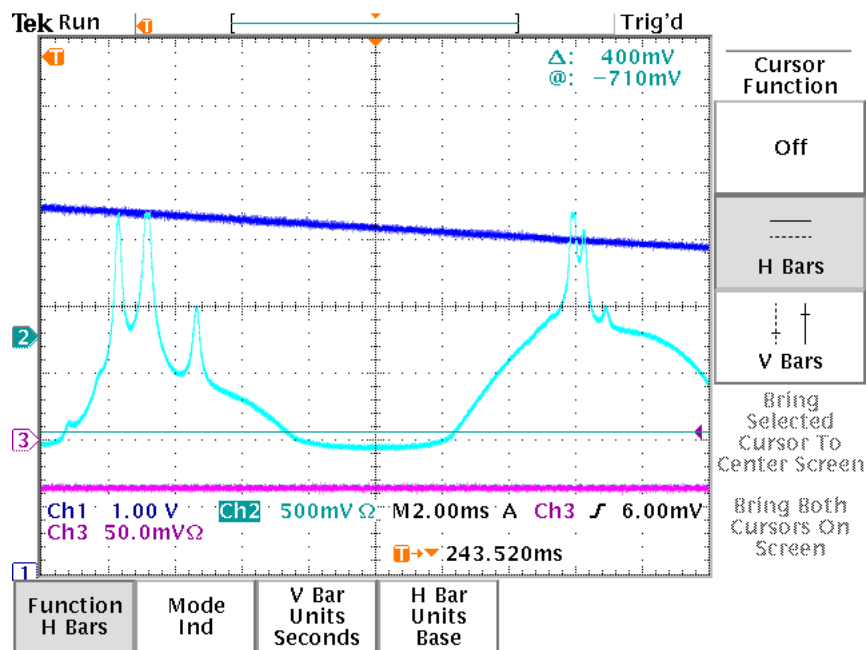Figure 12: A SAS spectrum with an aligned spectrometer

Figure 13: Hyperfine splitting of 85 and 87 rubidium $5P_{3/2}$ from left to right

5 Fabry-Pérot Interferometer

5.1 Brief Description

Like a Michelson interferometer, a Fabry-Pérot interferometer splits a beam from a (coherent) light source into separate paths of different optical distances, and recombines them afterwards.
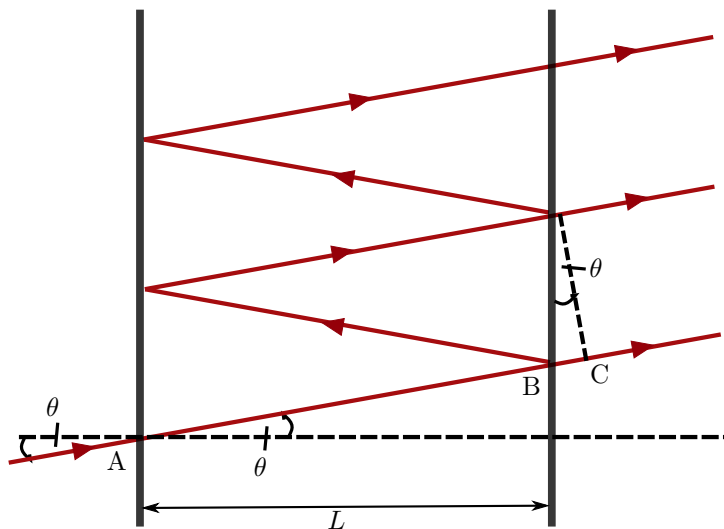

Figure 14: Beam paths in a Fabry-Pérot interferometer

The Fabry-Pérot interferometer consists of two high-reflecting mirrors, a distance L apart (fig. 14). We obtain constructive interference if the phase difference φ between two adjacent beams is a multiple of 2π. The phase difference is the ratio of the optical path length and the wavelength, multiplied by 2π,

$$\varphi = 2\pi \frac{s_{opt}}{\lambda}\,. \tag{4}$$

The difference of the optical paths of two neighboring beams is

$$s_{opt} = 2\,n_i\,\overline{AB} - n_o\,\overline{BC} = 2n_i\frac{L}{\cos\theta} - 2\,n_o\,L\tan\theta\,\sin\theta$$

$$= 2L\frac{n_i - n_o\,\sin^2\theta}{\cos\theta}\,, \tag{5}$$

where n_i and n_o are the indices of refraction between and outside of the two mirrors, respectively. Assuming $n_i = n_o = n$, eq. (5) simplifies to

$$s_{opt} = 2nL\cos\theta\,. \tag{6}$$

Therefore, the phase difference is

$$\varphi = \frac{4\pi}{\lambda}nL\cos\theta\,, \tag{7}$$

and constructive interference occurs for $\varphi = 2\pi\,m$ with integer m, i.e.

$$L = \frac{m\lambda}{2n\cos\theta} = \frac{mc}{2n\nu\cos\theta} \tag{8}$$

13

or

$$\nu_m = \frac{mc}{2nL\cos\theta} \,. \tag{9}$$

The distance between two peaks in the frequency spectrum is called the **free spectral range** (see fig. 15), and from eq. (9) we understand that it is given by

$$\Delta\nu_{\text{FSR}} = \frac{c}{2nL\cos\theta} \,. \tag{10}$$

In our case, the cavity length is large and the incident angle small, such that the approximation

$$\Delta\nu_{\text{FSR}} = \frac{c}{2nL} \tag{11}$$

is reasonable.

However, the TeachSpin interferometer utilized in this experiment uses two curved, confocal mirrors instead of plain ones, as it is illustrated in fig. 16. The effect is that any beam entering cavity is reflected to its original position after passing the cavity four times, compared to two times assuming plain mirrors. Thus the free spectral range in our case is

$$\Delta\nu_{\text{FSR}} = \frac{c}{4nL} \,. \tag{12}$$

For this to work properly, it is crucial that the mirrors are confocal, i.e. that the foci coincide exactly in the center of the cavity. The adjustment will be part of the alignment process.

The resolution of the interferometer also depends on the width of the peaks. If $\delta\nu$ is the full width at half maximum (FWHM, see also fig. 15), we define the **finesse** as

$$\mathcal{F} = \frac{\Delta\nu_{\text{FSR}}}{\delta\nu} \,. \tag{13}$$

According to the TeachSpin manual[2, p. 2], the cavity's finesse is over 100; we found that 65 was about best we could do.
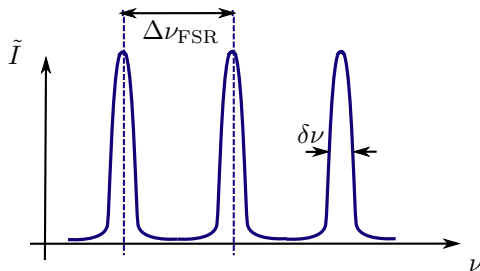

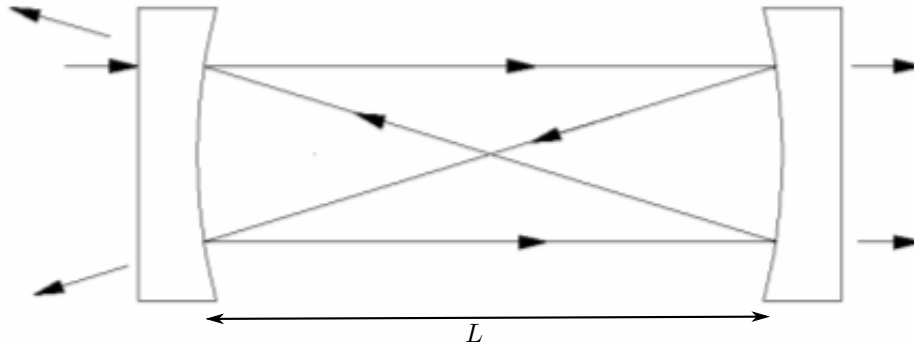Figure 15: Illustration of free spectral range and bandwidth

Figure 16: Sketch of a confocal-mirror Fabry-Pérot cavity[3]

5.2 Setup

The proper adjustment of the Fabry-Pérot interferometer is somewhat tricky. The instrument has very low tolerance regarding misalignment, but once you managed to figure it out, it rewards you with an enormous precision of frequency measurements.

We suggest to keep the one-beam absorption experiment and use the former pump beam as input to the interferometer. This allows for direct comparison of at least the Doppler-broadend spectrum with the interference pattern. You would not want to use the probe beam (or any low-intensity light) to run the interferometer because the output signal of the cavity is exceedingly weak. The transmittivity of the the mirrors is only about 0.5%.

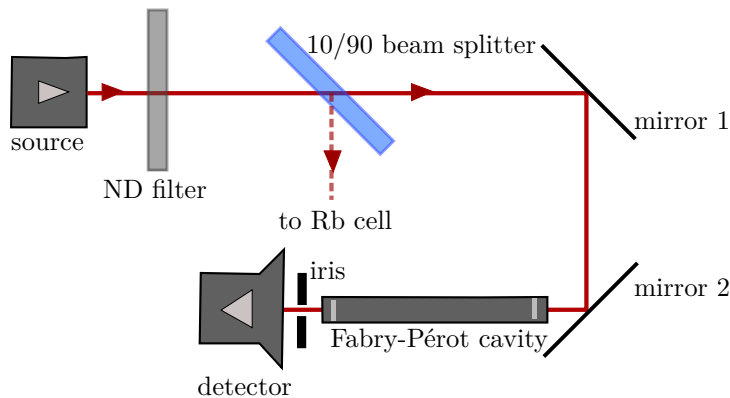For alignment, you may turn off the piezo ramp.

Figure 17: Setup for the Fabry-Pérot interferometry experiment

In the first step, you may try to get the beam going as straight as possible along the height of the optical axis of the cavity. You may adhere to the setup as in fig. 17, but leave out the cavity for the moment and

---

[3]Source: [2, p. 3]

replace the detector with a another mirror. Similarly to the previous alignments using a business card, you may now use the provided iris and the video camera to follow the beam path. Place the iris between mirrors 1 and 2, such that the hole is at the height of the optical axis of the cavity. Start with the iris close to mirror 2, and adjust mirror 1 to send the beam through the hole. Then move the iris close to mirror 1 and adjust mirror 2 to send the reflected beam through the hole, as well. Reduce the size of the iris and repeat these steps to achieve a better result.

Next, you may repeat the above steps for the path between mirror 2 and the detector mirror.

Once you made the incident and reflected beams collinear, you may restart the piezo ramp and bring the cavity and detector in place. Put the cavity close to mirror 2, and the detector should be placed right after the other end of the cavity. You might put the iris in between cavity and detector to have control over the light intensity reaching the detector.

You should be able to observe a signal similar to fig. 18(a) on the oscilloscope. The signal may or may not be inverted, depending on whether you connected the detector directly to the scope or via the inverting input of the op-amp. Note that you will have to increase the gain of the photodetector compared to previous experiments. A value between 1 and $10\,\mathrm{M\Omega}$ is reasonable.

If you zoom into the absorption spectrum, you will notice the zig-zag pattern of the signal (fig. 18(b)). Since the Fabry-Pérot cavity is transmitting in both directions, the filtered signal is fed back to the laser and affects the frequency in such a way that only discrete frequencies (matching with the resonance condition of the cavity) are eligible. So in this case, the misshaped absorption spectrum is actually indicating proper alignment.

To avoid the feedback, you may use a simple optical isolater consisting of a polarizer and a quarter-wave plate. Coming from the source, put first the polarizer and then the quarter-wave plate in the beam path. The polarizer's axis should be displaced by 45 degrees with respect to the quarter-wave plate's axes. Note that the laser light is already polarized, yet you may not know the polarization axis. You may try to adjust the axis of the polarizer to achieve maximum intensity. After passing the polarizer, the light is linearly polarized along its axis. With the quarter-wave plate at a 45 degrees angle, it changes the polarization to be circular. After the reflection at a perpendicular surface (here the mirror of the cavity), the polarization remains circular, but the handedness is reversed. Therefore, on its way back through the quarter-wave plate, the circular polarization is transformed back to a linear polarization, but at an angle of 90 degrees with respect to the original polarization, and thus the light cannot pass the polarizer. Since the provided quarter-wave plate is not precisely tuned to the $780\,\mathrm{nm}$ wavelength used in this experiment, you might have to tilt it a little to adjust the optical path.

With the optical isolater in place, the signal should look simliar to fig. 18(c). The resonance pattern of the cavity is still not symmetric, and the reason for this is that the two mirrors of the interferometer are not yet confocal. In fact, in fig. 18(c) we are on the falling edge of the scanning voltage ramp, and the grating sweep *increases* the laser frequency with time, i.e. the wavelength is decreased. Apparently, the tails of the peaks are stretched towards longer wavelengths, indicating that the cavity is too short. Therefore, you will have to twist the screws on both ends of the cavity to lengthen it. The signal should approach fig. 18(d). If you lengthen the cavity too much, the spectrum will stretch towards short wavelengths.

You may zoom in to a single peak and try to make it as symmetrical as possible. Slightly modify mirror 2 in fig. 17, and observe the change. You might be able to narrow the peak further. Measuring the full width at half maximum of a single peak and the distance between two resonances, you can now calculate the finesse of the cavity.

Our goal is to establish a relation between the piezo voltage and the laser frequency. One way to get there, similarly to the Michelson interferometer calibration, could be to measure the length of the cavity L and use eq. (12) for the free spectral range. Unfortunately, this is hardly possible with high accuracy. However, there is a more sophisticated, more precise way to reach a reference frequency, involving radio-frequency modulation of the laser light. In addition to the low-frequency ramp modulation of the laser current and
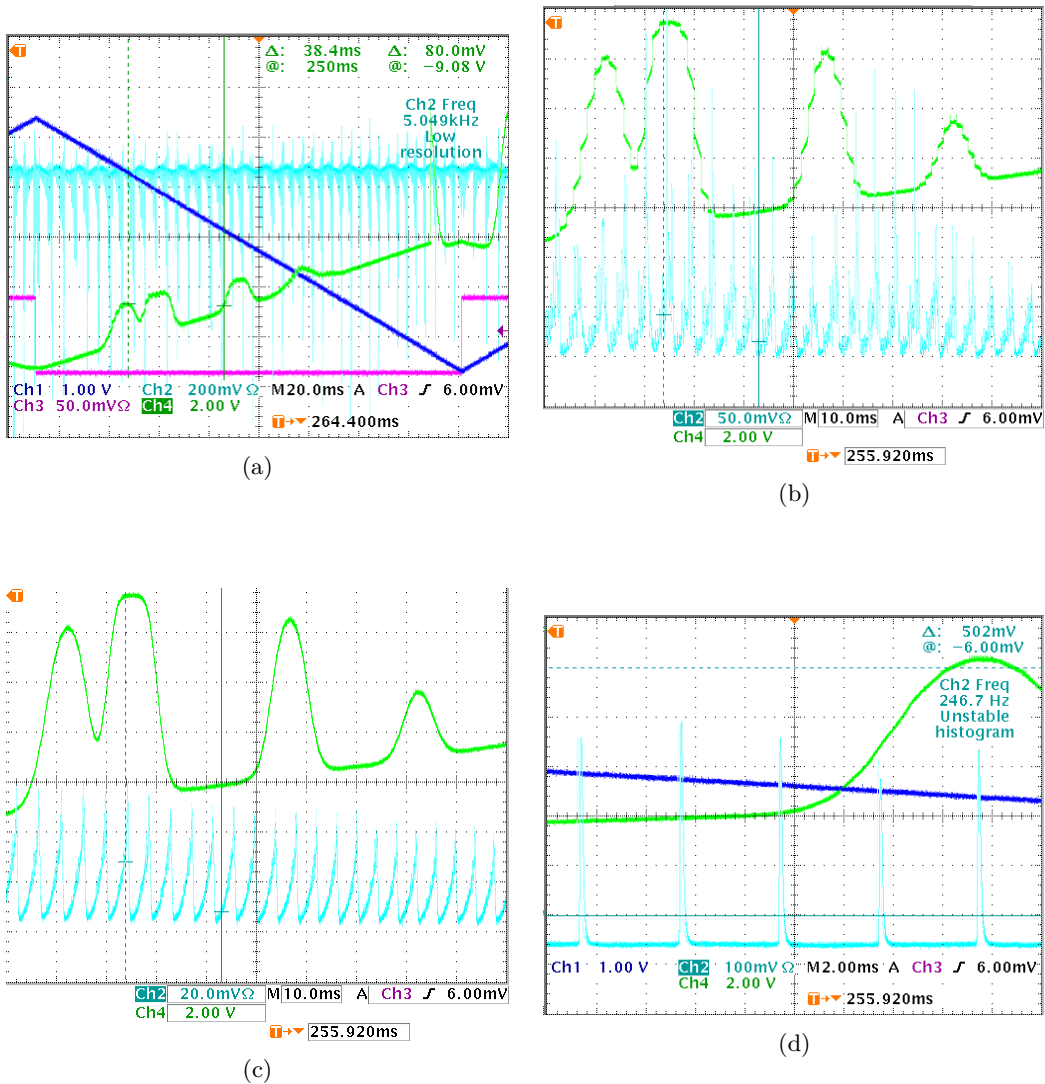
Figure 18: Adjustment of the Fabry-Pérot interferometer. (a) Fabry-Perot cavity transmission without optimization. (b) Influence of the cavity feedback to the absorption spectrum. (c) Reduced Feedback using a "poor-man's" optical isolator. (d) Optimized cavity length.
Blue: piezo voltage; turquois: cavity detector signal; green: Rb cell detector signal; pink: Trigger signal.

piezo voltage, we will add a known radio-frequency current modulation directly to the laser diode. Once we understand how this known rf modulation affects the laser spectrum, we will be able to read the ramp constant from the interferometer signal.

5.3 Frequency Modulation

In order to understand the effects of modulating the laser frequency, we consider a harmonic oscillation

$$g(t) = g_0 \cos(\omega t) \tag{14}$$

which in our case might be the electric field amplitude of the laser in a fixed direction at a fixed location (i.e. at the detector). By applying a radio-frequency modulation current to the diode, we effectively make the
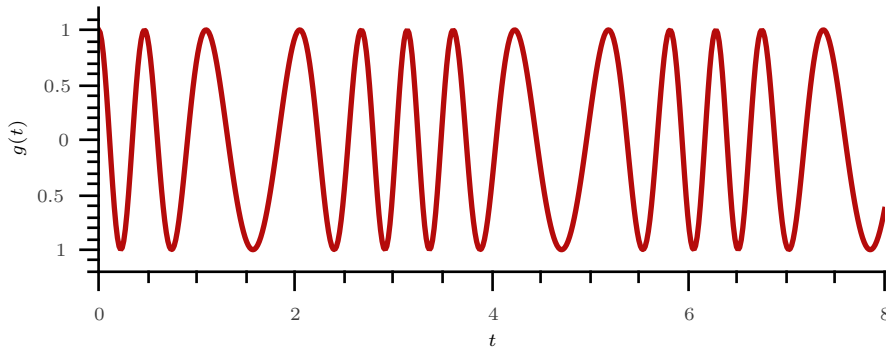
17

Figure 19: Example of a frequency modulated signal

frequency of the laser light time-dependent, $\omega \to \omega(t)$. We want to assume the modulation to be harmonic, too, i.e.

$$\omega(t) = \omega_0 + \hat{\omega} \cos(\omega_{rf} t). \tag{15}$$

In this expression, the *carrier frequency* ω_0 is the undisturbed frequency as it is selected by the diffraction grating angle, and ω_{rf} is the modulation frequency. Note that in the experiment, ω_0 is not a constant because we are scanning the laser frequency using the piezo controller. However, this scanning frequency is about $1\ldots10\,\mathrm{Hz}$, and is therefore small compared to the rf modulation frequency, such that we can assume it to be constant in the time scales considered. Finally, $\hat{\omega}$ is the modulation amplitude, defining the range around the carrier frequency in which the laser frequency is varied. To summarize, within a small time interval as compared to the scanning frequency, the laser frequency will oscillate harmonically between $\omega_0 - \hat{\omega}$ and $\omega_0 + \hat{\omega}$ with the oscillation frequency ω_{rf}. Fig. 19 gives an example of a frequency modulated signal.

Please also note table 1, which is to give an overview of the various frequencies involved in this discussion, and provides some typical values.

From eq. (15), we conclude that the phase of the signal is

$$\varphi(t) = \int_0^t \omega(t)\mathrm{d}t = \omega_0 t + \frac{\hat{\omega}}{\omega_{rf}} \sin(\omega_{rf} t), \tag{16}$$

symbol	name	description	typical value
ν_0; ω_0	carrier frequency	undisturbed laser frequency as selected by the diffraction grating angle and laser diode controller current	$384\,\mathrm{THz}$
$\hat{\nu}$; $\hat{\omega}$	modulation amplitude	range of frequencies covered by the rf current modulation	$1\,\mathrm{GHz}$
ν_{rf}; ω_{rf}	rf modulation frequency	frequency of the modulation current injected via the SMA connector directly at the laser diode	$10\,\mathrm{MHz}$
	scanning frequency	frequency of the ramp voltage signal used to sweep the diffraction grating angle within a certain range to select ν_0	$1\ldots10\,\mathrm{Hz}$
ν_{FP}	cavity resonance frequency	frequencies corresponding to a standing wave in the Fabry-Pérot cavity	$> 1\,\mathrm{GHz}$; here: $\approx 384\,\mathrm{THz}$

Table 1: Overview of the frequencies appearing in the description of the Fabry-Pérot interferometer
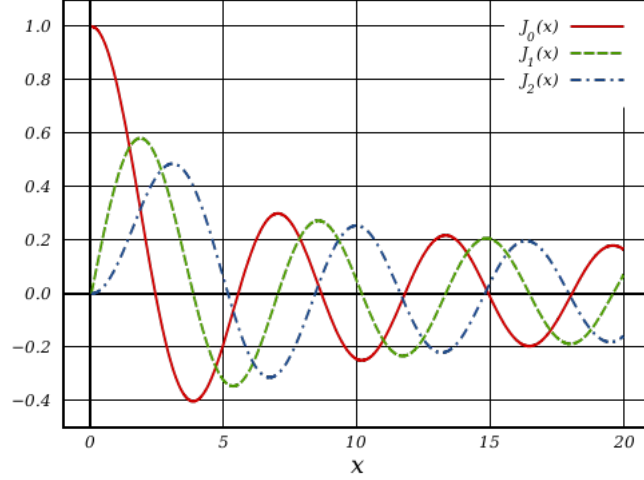
18

Figure 20: Bessel functions of the first kind for $n = 0, 2, 3$[4]

and using the modulation index $\eta = \frac{\hat{\omega}}{\omega_{rf}}$, the signal reads

$$g(t) = g_0 \cos(\varphi(t)) = g_0 \cos\left(\omega_0 t + \eta \sin(\omega_{rf} t)\right) = g_0 \operatorname{Re}\left[e^{-i(\omega_0 t + \eta \sin(\omega_{rf} t))}\right].$$ (17)

If $\omega_0 \gg \omega_{rf}$, the signal has the periodicity of the modulation signal. To obtain the frequency spectrum of g, we expand into a Fourier series,

$$g(t) = \operatorname{Re}\sum_{n=-\infty}^{\infty} \tilde{g}_n e^{-i\omega_n t},$$ (18)

where $\omega_n = \omega_0 + n\omega_{rf}$,

$$\text{and } \tilde{g}_n = \omega_{rf}\int_{-\pi/\omega_{rf}}^{\pi/\omega_{rf}} g(t) e^{i\omega_n t}dt = \omega_{rf} g_0 \int_{-\pi/\omega_{rf}}^{\pi/\omega_{rf}} e^{i(n\omega_{rf} t - \eta \sin(\omega_r f t))}dt = g_0 \int_{-\pi}^{\pi} e^{i(n\tau - \eta \sin(\tau))}d\tau.$$

Using the definition of the Bessel functions of the first kind[3] (compare fig. 20),

$$J_n(\eta) = \frac{1}{2\pi}\int_{-\pi}^{\pi} e^{i(n\tau - \eta \sin(\tau))}d\tau,$$ (19)

we finally obtain

$$g(t) = g_0 \operatorname{Re}\sum_{n=-\infty}^{\infty} J_n(\eta) e^{-i(\omega_0 + n\omega_{rf})t},$$ (20)

where a factor of 2π has been absorbed by the amplitude g_0.

We should take into account that a photodetector can only monitor intensities, such that the obtained signal in the experiment will actually be g^2. Furthermore, the Bessel functions of the first kind satisfy the relation

$$J_{-n}(\eta) = (-1)^n J_n(\eta).$$ (21)

We conclude that besides the original laser frequency $\nu_0 = \omega_0/2\pi$, we will also find peaks symmetrically around ν_0 at frequencies $\nu = \nu_0 \pm \nu_{rf}, \nu_0 \pm 2\nu_{rf}, \ldots$. Since $\eta = \hat{\omega}/\omega_{rf} = \hat{\nu}/\nu_{rf}$, the strength of the peaks depends on the amplitude of the modulation signal. By tuning η to the roots of J_n, one can suppress specific maxima in the frequency spectrum.

---

[4]Source: *http://en.wikipedia.org/wiki/Bessel_function*

at $t = t_0$

modulated laser light

$\tilde{I}$

Fabry-Pérot cavity

ν_0 ν_{FP}
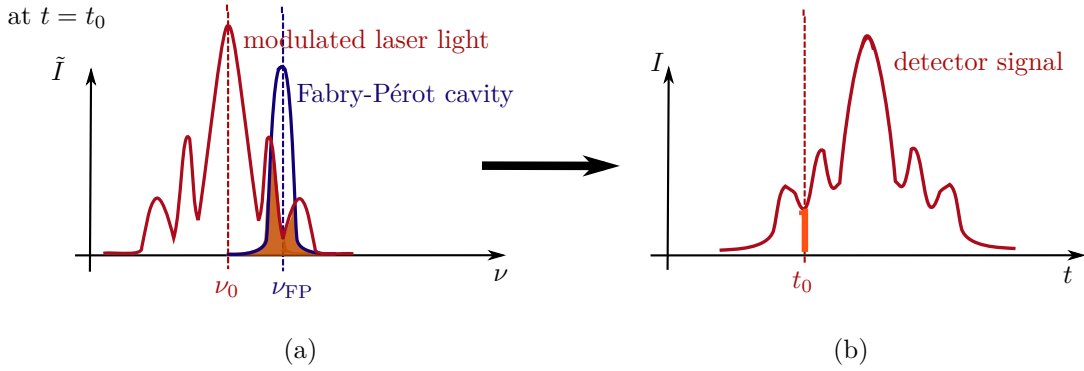
ν

(a)

I

detector signal

t_0

t

(b)

Figure 21: Monitoring the frequency spectrum in the time domain. (a) Spectrum in the frequency domain at a fixed time $t = t_0$, and (b) how it accounts for the corresponding component of the signal in the time domain.

5.4 Fabry-Pérot Cavity as a Fourier Transformer

It is quite amazing that the combination of the laser frequency scan and the sharp resonance peaks of the Fabry-Pérot cavity allow us to monitor the frequency spectrum of the modulated laser light in the time domain.

To understand how this works, we first note that the scanning frequency is between 1 and 10 Hz, whereas the laser modulation frequency might be of order 10 MHz. Therefore, we can assume the *carrier frequency ν_0*, i.e. the unmodulated laser frequency, to be constant at a specific point in time t_0. In other words, we assume that the piezo voltage scan *shifts* the whole frequency spectrum of the laser in time without modifying it.

You may consider fig. 21 now. In the frequency domain, the Fabry-Pérot cavity has a sharp resonance peak at ν_{FP} corresponding to a standing wave fitting into the cavity of length L. If the laser is not modulated, light will only pass through the cavity when $\nu_0 = \nu_{\mathrm{FP}}$, or rather $|\nu_0 - \nu_{\mathrm{FP}}| \lesssim \delta\nu$, where $\delta\nu$ is the bandwidth of the cavity.

Now let the laser be modulated by a radio-frequency current, such that the frequency spectrum of the laser light looks somewhat similar to the red curve in fig. 21(a). However, the cavity lets light pass only if its frequency is in the interval $\nu_{\mathrm{FP}} \pm \delta\nu$. Therefore, at $t = t_0$, of the original light with frequencies $\nu_0, \nu_0 \pm \nu_{rf}, \nu_0 \pm 2\nu_{rf} \ldots$, only parts with $\nu \approx \nu_{\mathrm{FP}}$ can reach the detector, which is the component of the frequency spectrum $\nu_0 - \nu_{\mathrm{FP}}$ away from the carrier frequency. If you look again at fig. 21(a), this corresponds to the overlap of the two curves (colored in orange), weighed by the frequency peak of the cavity (blue curve). So while the carrier frequency is slowly scanned through a certain range, the cavity "copies" the frequency spectrum to the time domain. Mathematically, this is a convolution of the laser signal with the cavity's frequency response function.

In the time domain (fig. 21(b)), the signal resembles the frequency spectrum of the cavity, but is slightly smoothed due to the non-zero bandwith $\delta\nu$ of the cavity.

5.5 Calibration of the Automated Frequency Scan Using the Fabry-Pérot Cavity

The knowledge of the spectrum of a frequency-modulated signal will allow you to improve your estimate of the piezo constant C_{ramp}, which established the relationship of the piezo voltage and the frequency changes according to eq. (3) above,

$$\Delta\nu = C_{\mathrm{ramp}}\Delta V \, . \tag{3}$$

By modulating the laser frequency with an rf current of frequency ν_{rf}, we expect to find maxima in the frequency spectrum which are a distance ν_{rf} apart from each other. By comparing the distance between two peaks with the change of the piezo voltage, we effectively measure C_{ramp}.

The laser current can be modulated directly through an SMA connector at the laser diode. Be extremely careful when walking through the following steps! The laser diode is exceedingly sensitive, and too high AC power may destroy it! Please also read the annotations on page 11 of the TeachSpin manual[2].

Leaving it unplugged from the laser diode, you may turn on the rf frequency generator and monitor the signal on the oscilloscope using the $50\,\Omega$ impedance. The suggested frequency range is $100\,\mathrm{kHz}$ to $500\,\mathrm{MHz}$. Examine the sensitivity of the generator's amplitude control. The amplitude must not exceed $0.7\,$volts peak-to-peak at any time.

Now you may attach the SMA to BNC adapter to the laser diode. Set the rf amplitude to zero and connect the laser with the generator. Carefully increase the amplitude, and watch the signal on the 'scope. Observe the changes of the cavity signal.

You shall notice that the main peak, belonging to the carrier frequency, will decrease, and two additional peaks left and right of it will emerge (fig. 22(a)). As you increase the rf amplitude further, more and more peaks will appear (fig. 22(b)). Also, you might discover that certain peaks vanish and reappear from time to time. This effect is due to the Bessel function modulation described above (eq. (20)). Whenever the ratio of the modulation range and the rf frequency, $\hat{\nu}/\nu_{rf}$, reaches a root of the nth Bessel function, the corresponding peaks will disappear!
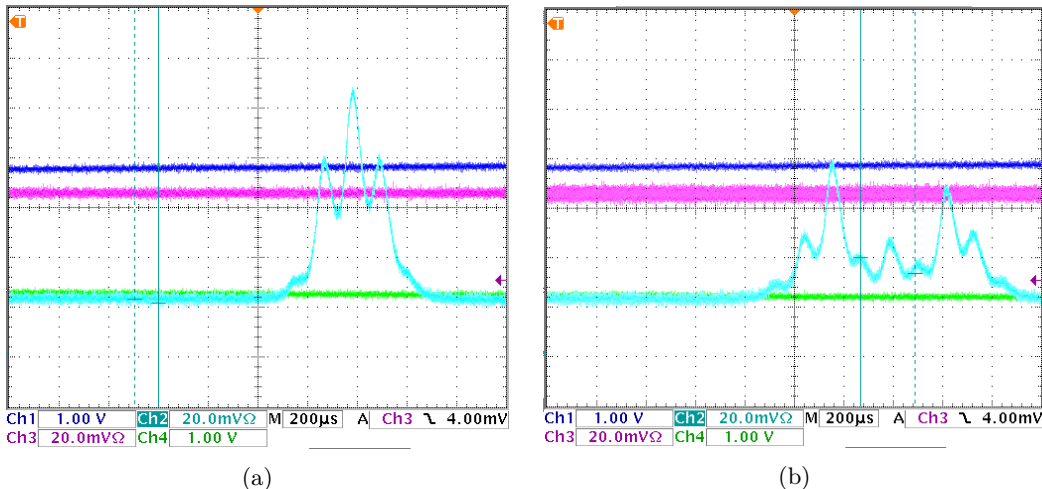

| Ch1 | 1.00 V | Ch2 | 20.0mVΩ | M 200μs | A | Ch3 | 4.00mV |
| Ch3 | 20.0mVΩ | Ch4 | 1.00 V | | | | |

(a)

| Ch1 | 1.00 V | Ch2 | 20.0mVΩ | M 200μs | A | Ch3 | 4.00mV |
| Ch3 | 20.0mVΩ | Ch4 | 1.00 V | | | | |

(b)

Figure 22: Spectrum of modulated laser light, carrier frequency $\nu_0 \approx 380\,\mathrm{GHz}$, modulation frequency $\nu_{rf} = 10.9\,\mathrm{MHz}$. (a) rf amplitude $V_{rf} = 145\,\mathrm{mV_{pp}}$. (b) rf amplitude $V_{rf} = 345\,\mathrm{mV_{pp}}$.

Knowing the distance between the peaks, you can now correlate the frequency change $\Delta\nu$ to a difference in scanning time Δt_ν. Comparing this to the change of the piezo voltage ΔV per time Δt_V, you can calculate the ramp constant C_{ramp}. You may use this value to examine the hyperfine splitting of the $5S_{1/2}$ and (if possible) $5P_{3/2}$ levels of both rubidium isotopes from your saturated absorption experimental data.

References

[1] User's Manual for *Diode Laser Spectroscopy, DLS1-A*.
    TeachSpin, Inc., Buffalo, NY, Rev. 2.0 11/09.

[2] Instructor's Manual for *Fabry-Perot Cavity, FP1-A*.
    TeachSpin, Inc., Buffalo, NY, Rev. 2.0 11/09.

[3] *NIST Digital Library of Mathematical Functions.*
    National Institute of Standards and Technology.
    Chapter 10 Bessel Functions: *http://dlmf.nist.gov/10*, access: 12/04/2013.

A Example: Identification and Measurement of $5S_{1/2}$ Hyperfine Splitting

Using the ramp constant C_{ramp} and an absorption spectrum obtained from the oscilloscope it is possible to quantify hyperfine splitting of in this scenario $5S_{1/2}$ levels.
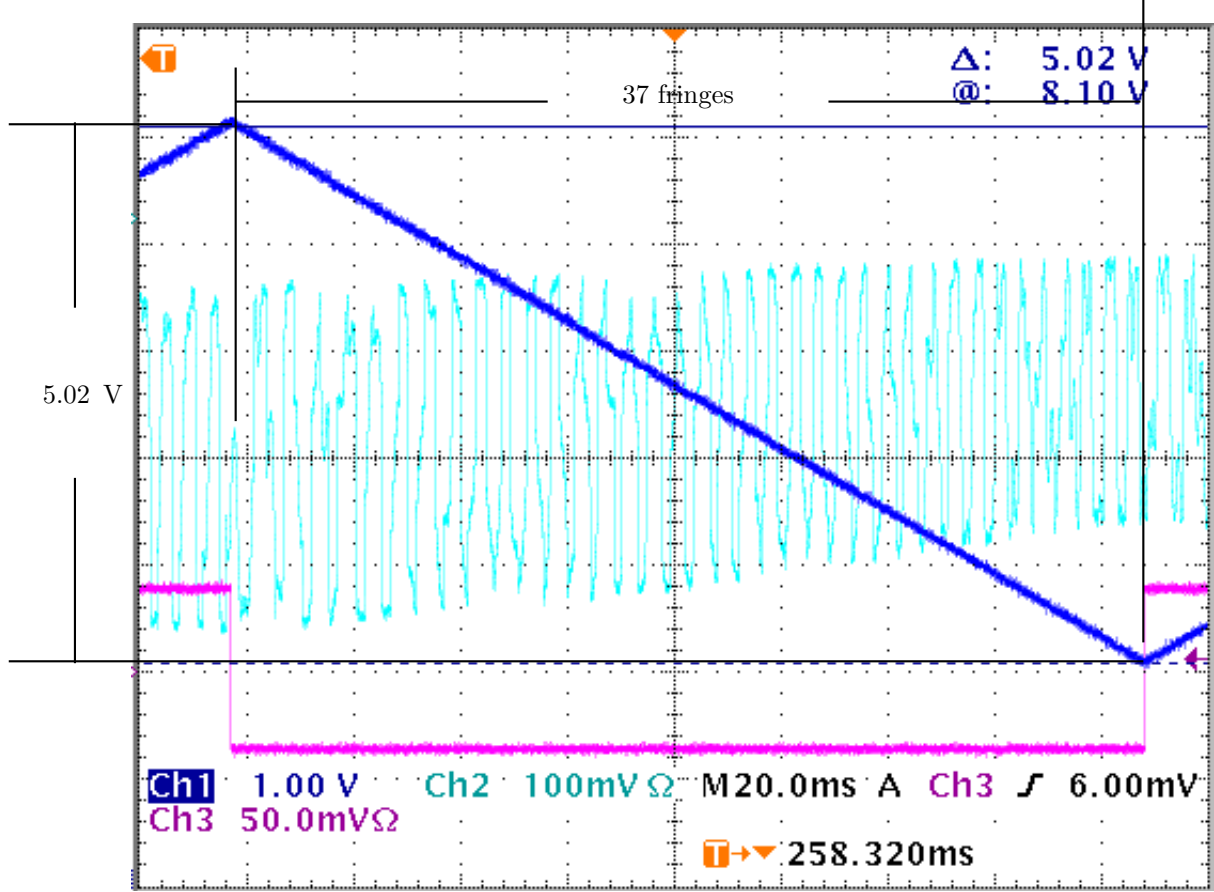

Figure 23: Determination of C_{ramp} from the Michelson interferometry experiment

Figure 23 demonstrates how to extract C_{ramp} using equation 3 wherein:

$$C_{\text{ramp}} = \frac{c}{\delta \, V_m}, \qquad V_m = \Delta V/\Delta m, \qquad \delta = 2|L_1 - L_2|$$

$$L_1 = 0.052 \pm 0.002\,\text{m}, \quad L_2 = 0.402 \pm 0.002\,\text{m}, \quad \Delta m = 37, \quad \Delta V = 5.02 \pm 0.05\,\text{V}$$

$$\Rightarrow \quad C_{\text{ramp}} = 3.2 \pm 0.05\,\text{Ghz/V}$$

Error incurred in this calculation is primarily due to the length measurement $\pm 2\,\text{mm}$, and the voltage measurement $\pm 0.05\,\text{V}$. Analysis of a single beam absorption spectrum is shown in figure 24. Change in voltage was extracted from the oscilloscope image and is likely subject to random error of $\pm 0.1\,\text{V}$. From figure 24 hyperfine splitting is recorded in table 2.
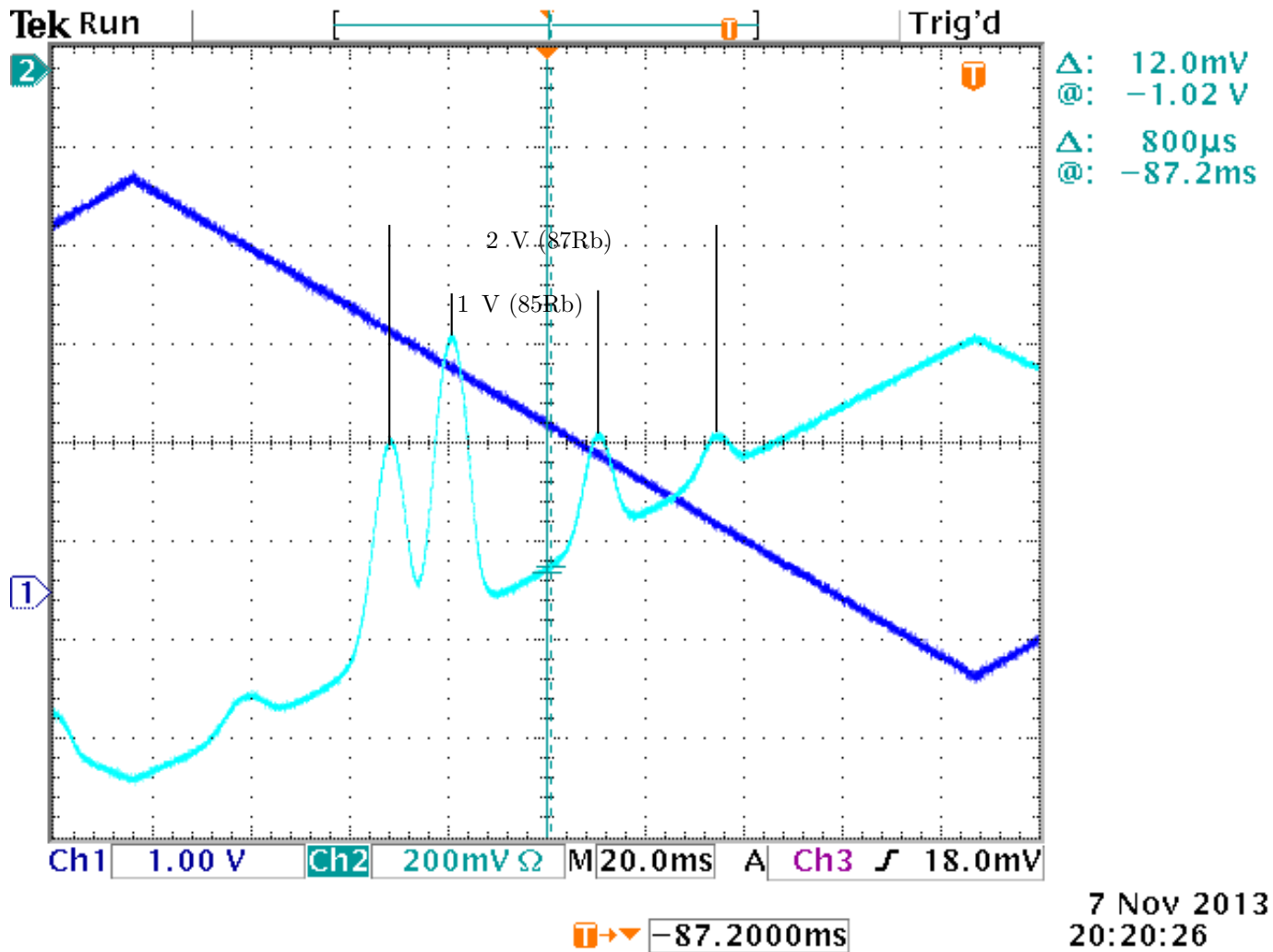
Figure 24: Single beam absorption spectrum identifying hyperfine splitting for 87 and 85 rubidium.

Isotope	Measurement GHz	Theory GHz
85	3.2 ± 0.12	3.03
87	6.4 ± 0.066	6.84

Table 2: Measurement of hyperfine splitting in two isotopes of rubidium when using a single beam absorption

B   Example: Determining the Fabry-Pérot Cavity's Finesse

In order to find the finesse of the Fabry-Pérot cavity for an optimized configuration, we obtained two datasets to measure the free spectral range and the bandwidth separately. Both datasets were recorded using the same settings for the frequency sweep, such that the ratio of the times corresponding to the free spectral range and the bandwidth resembles the ratio of the quantities in the frequency domain. More precisely,

$$\Delta \nu_{\text{FSR}} = C_{\text{ramp}} \Delta V_{\text{FSR}} = C_{\text{ramp}} \Delta t_{\text{FSR}} \frac{\Delta V_{\text{ramp}}}{\Delta t_{\text{ramp}}} \,, \tag{22}$$
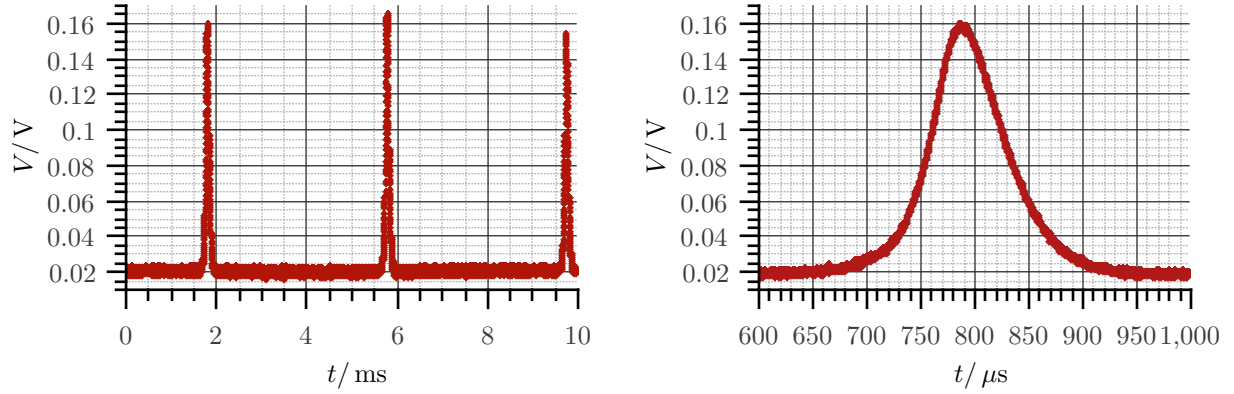
Figure 25: Fabry-Pérot cavity transmission. Both datasets were obtained using the same frequency scan settings, i.e. the same modulation ramp for laser current and piezo voltage. Left: Range of peaks to determine free spectral range. Right: Single peak to measure bandwidth.

and

$$\delta\nu = C_{\mathrm{ramp}}\Delta V_{\delta\nu} = C_{\mathrm{ramp}}\Delta t_{\delta\nu}\frac{\Delta V_{\mathrm{ramp}}}{\Delta t_{\mathrm{ramp}}}\,,$$

such that

$$\mathcal{F} = \frac{\Delta\nu_{\mathrm{FSR}}}{\delta\nu} = \frac{\Delta t_{\mathrm{FSR}}}{\Delta t_{\delta\nu}}\,.$$

From the datasets plotted in fig. 25, we find

$$2\Delta t_{\mathrm{FSR}} = (7.937 \pm 0.004)\,\mathrm{ms}\,,$$

corresponding to the difference between the two outer peaks, and

$$\Delta t_{\delta\nu} = (82.3 \pm 3.0)\,\mu\mathrm{s}$$

for the full width at half maximum; maximum voltage is $(0.160 \pm 0.005)\,\mathrm{V}$ at $(791.2 \pm 1.5)\,\mu\mathrm{s}$. This yields a finesse of

$$\mathcal{F} = \frac{\Delta t_{\mathrm{FSR}}}{\Delta t_{\delta\nu}} = 48 \pm 2\,.$$

Using the calibration of the frequency scan as it is done in appendix C, we can also calculate the free spectral range of the cavity, finding from eq. (22):

$$\Delta\nu_{\mathrm{FSR}} = 379\,\mathrm{MHz}\,.$$

Comparing with eq. (12), we obtain a cavity length of

$$L = 19.8\,\mathrm{cm}\,,$$

which is in conformance with the dimension of the apparatus and the value quoted in the TeachSpin manual[2, p. 2].

C Example: Calibrating the Frequency Scan Using the Fabry-Pérot Cavity

Following the description of section 5, a radio-frequency current is used to modulate the laser light. The combined piezo voltage/laser current sweep scans the frequency spectrum.

Modulation data:

- scanning rate (ramp frequency): $3\,\mathrm{Hz}$

- rf modulation frequency: $\nu_{rf} = (10.9 \pm 0.1)\,\mathrm{MHz}$
  (calculated from period $T_{rf} = (92 \pm 1)\,\mathrm{ns}$)

- rf modulation amplitude: $V_{rf} = (345 \pm 5)\,\mathrm{V_{pp}}$

Maxima of intensity (from data set, see also fig. 26):

order	V/V	$t/\mu\mathrm{s}$	$\delta t/\mu\mathrm{s}$	$\Delta t_0/\mu\mathrm{s}$	$\delta\Delta t_0/\mu\mathrm{s}$
-3	0.0500	1042	10	347	13
-2	0.0760	1157	6	232	10
-1	0.0408	1264	10	125	13
0	0.0468	1389	8	0	11
1	0.0384	1506	10	117	13
2	0.0688	1621	6	232	10
3	0.0500	1726	8	337	11
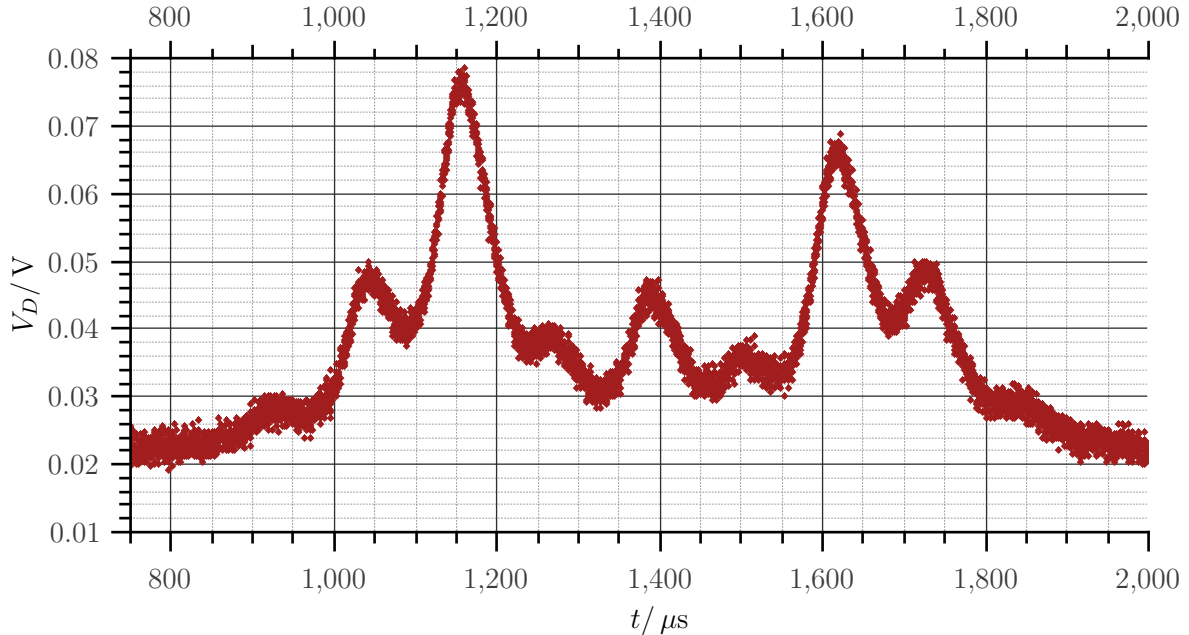
Figure 26: Frequency spectrum of $780\,\mathrm{nm}$ laser light, modulated at $\nu_{rf} = 10.9\,\mathrm{MHz}$, using Fabry-Pérot interferometer

Taking outermost maxima with $t_\nu = (684 \pm 18)\,\mu s$ corresponding to $\Delta\nu = 6\nu_{rf} = (65.4 \pm 0.6)\,\mathrm{MHz}$ yields

$$\frac{\Delta\nu}{\Delta t_\nu} = (95.6 \pm 2.7)\,\mathrm{GHz/s}\,. \tag{23}$$

For the ramp voltage, we find $\Delta V_{\mathrm{ramp}} = (5.00 \pm 0.05)\,\mathrm{V}$ for $\Delta t_{\mathrm{ramp}} = (170 \pm 5)\,\mathrm{ms}$, i.e.

$$\frac{\Delta V_{\mathrm{ramp}}}{\Delta t_{\mathrm{ramp}}} = (29.4 \pm 0.9)\,\mathrm{V/s}\,. \tag{24}$$

Finally,

$$C_{\mathrm{ramp}} = \frac{\Delta\nu}{\Delta V_{\mathrm{ramp}}} = \frac{\Delta\nu}{\Delta t_\nu}\frac{\Delta t_{\mathrm{ramp}}}{\Delta V_{\mathrm{ramp}}} = (3.25 \pm 0.14)\,\mathrm{GHz/V}\,. \tag{25}$$

D   Example: Calculating the Hyperfine Splitting

Using the calibration data from appendix C, we calculate the hyperfine splitting of rubidium. The saturated absorption data used in this calculation is plotted in fig. 27. Close-ups are given in fig. 28.

Let us first clarify our expectations. The dataset was acquired from the falling slope of the ramp voltage used to scan the diffraction grating angle and laser current. As discussed above, this means that the laser frequency increases in time. From fig. 1 we learn that we should find four "main areas" of resonance corresponding to the hyperfine splitting of the ground states of the 87Rb and 85 Rb isotopes. These areas of resonance resemble the single beam absorption spectrum. Since the frequencies are scanned from low to high, we conclude that the peaks belong to the 87Rb $F = 2$, 85Rb $F = 3$, 85Rb $F = 2$, 87Rb $F = 1$ levels (from left to right).

The Zeeman splitting due to the Earth's magnetic field produces transition frequencies of about $1\ldots 10\,\mathrm{MHz}$, so we can disregard any magnetic effects in this experiment. Hence, from fig. 1 we expect to find up to four resonances per resonance area, resembling the hyperfine splitting of the $5P_{3/2}$ levels. In practice, the selection
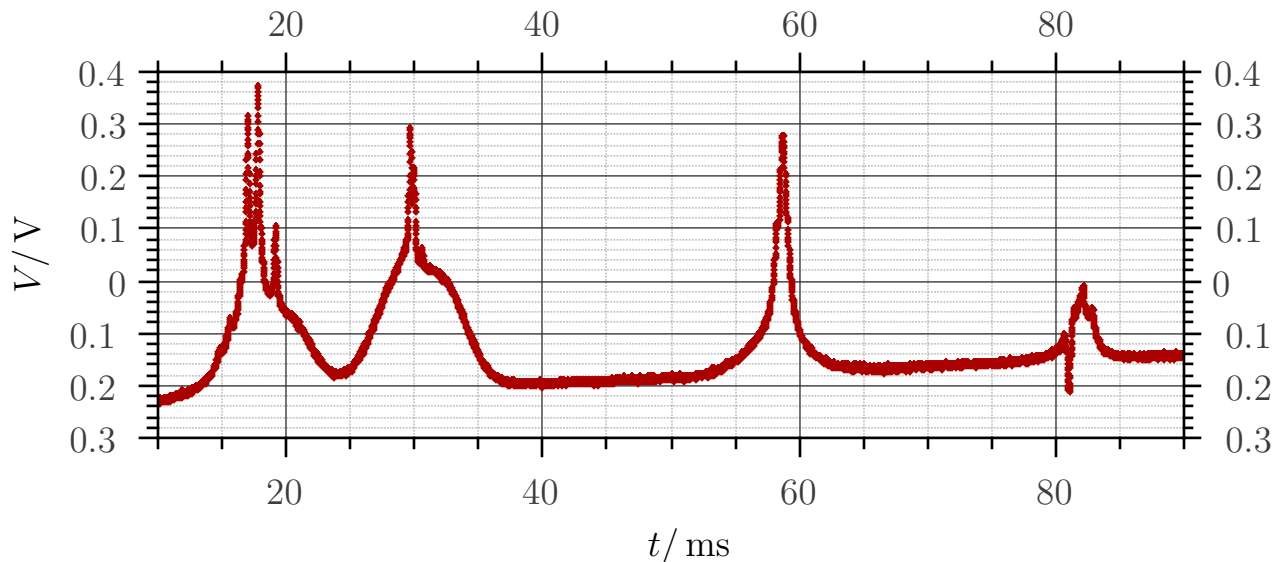

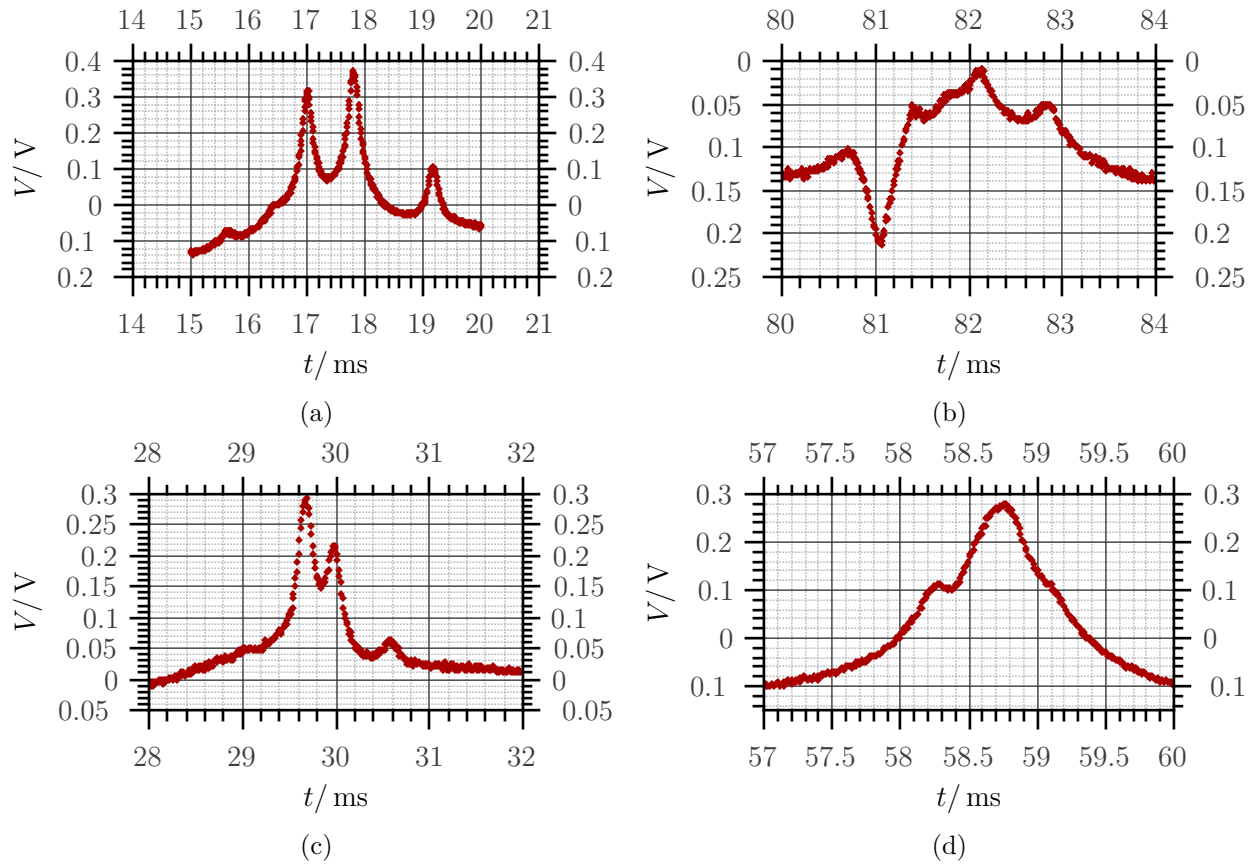Figure 27: Resonance spectrum of rubidium in saturated absorption experiment

Figure 28: Close-ups of the resonance areas corresponding to the 87Rb and 85Rb isotopes' ground states. (a) 87Rb, $F = 2$; (b) 87Rb, $F = 1$; (c) 85Rb, $F = 3$; (d) 85Rb, $F = 2$.

rules for optical transitions will put a constraint on the observed resonances; in general, only transitions with $\Delta F = 0, \pm 1$ are probable.

A linear fit of the falling slope of the ramp voltage gives

$$\frac{\Delta V_{\mathrm{ramp}}}{\Delta t_{\mathrm{ramp}}} = (29.7 \pm 0.2)\,\mathrm{V/s}\,; \tag{26}$$

this constant in combination with C_{ramp} as in appendix C will be used to calculate the frequency differences of the peaks from their distance in time.

The first thing we note is that the average distances between the 87Rb and 85Rb ground states are 65 ms and 28 ms, respectively, which lead to hyperfine splittings of the ground states of 6.3 GHz and 2.7 GHz. Comparing to the reference values of 6.8 GHz and 3.0 GHz we notice that the ratio of the two splitting frequencies is about the same. This suggests a systematic error of the ramp constant of about 10%. Therefore, we will also consider a corrected ramp constant C_{ramp}^* in our analysis, which is determined to be

$$C_{\mathrm{ramp}}^* = 3.55\,\mathrm{GHz/V}$$

to account for average ground state hyperfine splittings of 6.85 GHz for 87Rb and 2.95 GHz for 85Rb.

We obtain the following results, where $\Delta\nu$ is the frequency difference between the peaks using C_{ramp}, and $\Delta\nu_{\mathrm{corr}}$ is the frequency difference using C_{ramp}^*:

- 87Rb, $F = 2$ (fig. 28(a)):

Peak	$t/\,\mathrm{ms}$	$\delta t/\,\mathrm{ms}$	$(t_n - t_{n-1})/\,\mathrm{ms}$	$\Delta\nu/\,\mathrm{GHz}$	$\delta\Delta\nu/\,\mathrm{GHz}$	$\Delta\nu_{\mathbf{corr}}/\,\mathrm{GHz}$
(1)	15.65	0.10				
(2)	16.45	0.10	0.80	0.077	0.014	0.084
3	17.02	0.01	0.57	0.055	0.010	0.060
4	17.81	0.01	0.79	0.077	0.004	0.084
5	19.17	0.01	1.36	0.131	0.006	0.143

- 87Rb, $F = 1$ (fig. 28(b)):

Peak	$t/\,\mathrm{ms}$	$\delta t/\,\mathrm{ms}$	$(t_n - t_{n-1})/\,\mathrm{ms}$	$\Delta\nu/\,\mathrm{GHz}$	$\delta\Delta\nu/\,\mathrm{GHz}$	$\Delta\nu_{\mathbf{corr}}/\,\mathrm{GHz}$
(1)	81.05	0.05				
2	81.40	0.05	0.35	0.034	0.007	0.037
3	17.02	0.10	0.70	0.068	0.011	0.074
4	17.81	0.10	0.75	0.072	0.014	0.079

- 85Rb, $F = 3$ (fig. 28(c)):

Peak	$t/\,\mathrm{ms}$	$\delta t/\,\mathrm{ms}$	$(t_n - t_{n-1})/\,\mathrm{ms}$	$\Delta\nu/\,\mathrm{GHz}$	$\delta\Delta\nu/\,\mathrm{GHz}$	$\Delta\nu_{\mathbf{corr}}/\,\mathrm{GHz}$
1	29.69	0.01				
2	29.98	0.02	0.30	0.028	0.003	0.031
3	30.56	0.10	0.58	0.056	0.010	0.061

- 85Rb, $F = 2$ (fig. 28(d)):

Peak	$t/\,\mathrm{ms}$	$\delta t/\,\mathrm{ms}$	$(t_n - t_{n-1})/\,\mathrm{ms}$	$\Delta\nu/\,\mathrm{GHz}$	$\delta\Delta\nu/\,\mathrm{GHz}$	$\Delta\nu_{\mathbf{corr}}/\,\mathrm{GHz}$
1	58.30	0.05				
2	58.75	0.05	0.45	0.043	0.007	0.047

Unfortunately, neither the original C_{ramp} nor the corrected C_{ramp}^* yield results that match the theoretical expectations. The obtained frequencies seem to be too small. Besides, at least for the 87Rb we find more resonance peaks than expected from the above considerations, although the first peaks (in parentheses in the table) are either considerably weaker ($F = 2$) or might be caused by a mode hop ($F = 1$).

However, we may draw a qualitative conclusion finding that the areas of higher angular momentum in the ground state show higher frequency differences in the excited states, resembling the selection rules.

E   Instruments Used in the Experiments

Laser:

- *TeachSpin Diode Laser*

- Laser diode controller for laser temperature and current, diffraction grating angle, detector signal amplifier: *TeachSpin Laser Diode Controller*

- Monitors of laser parameters: *FLUKE 45 Dual Display Multimeter*

Optical Components:

- *TachSpin Fabry-Pérot Cavity* $780 \pm 40\,\text{nm}$

- Other optical components (mirrors, beam splitters, photodetectors, polarizers, quarter-wave plates): *TeachSpin*

Rubidium Cell:

- *TeachSpin Rubidium Cell with Helmholtz Coils*

- Temperature control of rubidium cell: *TeachSpin Laser Diode Controller*

- Coil current supply: *MPJA DC POWER SUPPLY HZ 5003*

Signal Processing:

- Oscilloscope (signal monitor): *Tektronix TDS 3024B*

- Frequency generator (rf): *Hewlett Packard 3312A Function Generator*

- Video camera (CCD): *TeachSpin*

- Video monitor: *COBY CX-TV1*

Contents